Biomedical Optics EXPRESS

Optical coherence tomography for the identification of musculoskeletal structures of the spine: a pilot study

Kathy Beaudette,[1,3] Mathias Strupler,[1,3] Fouzi Benboujja,[1,3] Stefan Parent,[3] Carl-Eric Aubin,[2,3] and Caroline Boudoux[1,3,*]

[1]*Engineering Physics Department, École Polytechnique de Montréal, P.O. Box 6079, Station Centre-ville, Montreal, Quebec, Canada*

[2]*Mechanical Engineering Department, École Polytechnique de Montréal, P.O. Box 6079, Station Centre-ville, Montreal, Quebec, Canada*

[3]*Sainte-Justine University Hospital Center, 3175, Côte Sainte-Catherine Road, Montreal, Quebec, Canada*

**caroline.boudoux@polymtl.ca*

Abstract: Adolescent idiopathic scoliosis (AIS) is a complex three-dimensional deformity of the spine requiring in severe cases invasive surgery. Here, we explore the potential of optical coherence tomography (OCT) as a guiding tool for novel fusionless minimally invasive spinal surgeries on an ex vivo porcine model. We show that OCT, despite its limited penetration depth, may be used to precisely locate structures such as growth plate, bone and intervertebral disk using relative attenuation coefficients. We further demonstrate a segmentation algorithm that locates growth plates automatically on *en-face* OCT reconstructions.

OCIS codes: (170.3660) Light propagation in tissues; (170.3880) Medical and biological imaging; (170.4500) Optical coherence tomography; (170.6935) Tissue characterization.

References and links

1. E. J. Wall, D. I. Bylski-Austrow, R. J. Kolata, and A. H. Crawford, "Endoscopic mechanical spinal hemiepiphysiodesis modifies spine growth," Spine **30**(10), 1148–1153 (2005).
2. R. R. Betz, A. Ranade, A. F. Samdani, R. Chafetz, L. P. D'Andrea, J. P. Gaughan, J. Asghar, H. Grewal, and M. J. Mulcahey, "Vertebral body stapling: a fusionless treatment option for a growing child with moderate idiopathic scoliosis," Spine **35**(2), 169–176 (2010).
3. J. T. Braun, E. Akyuz, J. W. Ogilvie, and K. N. Bachus, "The efficacy and integrity of shape memory alloy staples and bone anchors with ligament tethers in the fusionless treatment of experimental scoliosis," J. Bone Joint Surg. Am. **87**(9), 2038–2051 (2005).
4. M. Driscoll, C.-E. Aubin, A. Moreau, Y. Wakula, J. F. Sarwark, and S. Parent, "Spinal growth modulation using a novel intravertebral epiphyseal device in an immature porcine model," Eur. Spine J. **21**(1), 138–144 (2012).
5. P. O. Newton, V. V. Upasani, C. L. Farnsworth, R. Oka, R. C. Chambers, J. Dwek, J. R. Kim, A. Perry, and A. T. Mahar, "Spinal growth modulation with use of a tether in an immature porcine model," J. Bone Joint Surg. Am. **90**(12), 2695–2706 (2008).
6. E. C. Schmid, C. E. Aubin, A. Moreau, J. Sarwark, and S. Parent, "A novel fusionless vertebral physeal device inducing spinal growth modulation for the correction of spinal deformities," Eur. Spine J. **17**(10), 1329–1335 (2008).
7. J. S. Price, B. O. Oyajobi, and R. G. Russell, "The cell biology of bone growth," Eur. J. Clin. Nutr. **48**(Suppl 1), S131–S149 (1994).
8. D. Huang, E. A. Swanson, C. P. Lin, J. S. Schuman, W. G. Stinson, W. Chang, M. R. Hee, T. Flotte, K. Gregory, C. A. Puliafito, and J. G. Fujimoto, "Optical coherence tomography," Science **254**(5035), 1178–1181 (1991).
9. G. J. Tearney, M. E. Brezinski, B. E. Bouma, S. A. Boppart, C. Pitris, J. F. Southern, and J. G. Fujimoto, "In vivo endoscopic optical biopsy with optical coherence tomography," Science **276**(5321), 2037–2039 (1997).
10. S. B. Adams, Jr., P. R. Herz, D. L. Stamper, M. J. Roberts, S. Bourquin, N. A. Patel, K. Schneider, S. D. Martin, S. Shortkroff, J. G. Fujimoto, and M. E. Brezinski, "High-resolution imaging of progressive articular cartilage degeneration," J. Orthop. Res. **24**(4), 708–715 (2006).
11. D. M. Bear, A. Williams, C. T. Chu, C. H. Coyle, and C. R. Chu, "Optical coherence tomography grading correlates with MRI T2 mapping and extracellular matrix content," J. Orthop. Res. **28**(4), 546–552 (2010).
12. C. R. Chu, N. J. Izzo, J. J. Irrgang, M. Ferretti, and R. K. Studer, "Clinical diagnosis of potentially treatable early articular cartilage degeneration using optical coherence tomography," J. Biomed. Opt. **12**(5), 051703 (2007).

#160161 - $15.00 USD Received 19 Dec 2011; revised 1 Feb 2012; accepted 4 Feb 2012; published 13 Feb 2012

13. W. Drexler, D. Stamper, C. Jesser, X. Li, C. Pitris, K. Saunders, S. Martin, M. B. Lodge, J. G. Fujimoto, and M. E. Brezinski, "Correlation of collagen organization with polarization sensitive imaging of in vitro cartilage: implications for osteoarthritis," J. Rheumatol. **28**(6), 1311–1318 (2001).
14. C. W. Han, C. R. Chu, N. Adachi, A. Usas, F. H. Fu, J. Huard, and Y. Pan, "Analysis of rabbit articular cartilage repair after chondrocyte implantation using optical coherence tomography," Osteoarthritis Cartilage **11**(2), 111–121 (2003).
15. J. M. Herrmann, C. Pitris, B. E. Bouma, S. A. Boppart, C. A. Jesser, D. L. Stamper, J. G. Fujimoto, and M. E. Brezinski, "High resolution imaging of normal and osteoarthritic cartilage with optical coherence tomography," J. Rheumatol. **26**(3), 627–635 (1999).
16. X. Li, S. Martin, C. Pitris, R. Ghanta, D. L. Stamper, M. Harman, J. G. Fujimoto, and M. E. Brezinski, "High-resolution optical coherence tomographic imaging of osteoarthritic cartilage during open knee surgery," Arthritis Res. Ther. **7**(2), R318–R323 (2005).
17. Y. Pan, Z. Li, T. Xie, and C. R. Chu, "Hand-held arthroscopic optical coherence tomography for in vivo high-resolution imaging of articular cartilage," J. Biomed. Opt. **8**(4), 648–654 (2003).
18. J. Aerssens, S. Boonen, G. Lowet, and J. Dequeker, "Interspecies differences in bone composition, density, and quality: potential implications for in vivo bone research," Endocrinology **139**(2), 663–670 (1998).
19. R. A. McLaughlin, L. Scolaro, P. Robbins, C. Saunders, S. L. Jacques, and D. D. Sampson, "Parametric imaging of cancer with optical coherence tomography," J. Biomed. Opt. **15**(4), 046029 (2010).
20. F. J. van der Meer, D. J. Faber, D. M. B. Sassoon, M. C. Aalders, G. Pasterkamp, and T. G. van Leeuwen, "Localized measurement of optical attenuation coefficients of atherosclerotic plaque constituents by quantitative optical coherence tomography," IEEE Trans. Med. Imaging **24**(10), 1369–1376 (2005).
21. C. Xu, J. M. Schmitt, S. G. Carlier, and R. Virmani, "Characterization of atherosclerosis plaques by measuring both backscattering and attenuation coefficients in optical coherence tomography," J. Biomed. Opt. **13**(3), 034003 (2008).
22. U. Sharma, E. W. Chang, and S. H. Yun, "Long-wavelength optical coherence tomography at 1.7 microm for enhanced imaging depth," Opt. Express **16**(24), 19712–19723 (2008).
23. V. M. Kodach, J. Kalkman, D. J. Faber, and T. G. van Leeuwen, "Quantitative comparison of the OCT imaging depth at 1300 nm and 1600 nm," Biomed. Opt. Express **1**(1), 176–185 (2010).

1. Introduction

Adolescent idiopathic scoliosis (AIS) is a complex three-dimensional deformity of the spine requiring surgery in severe cases. Traditional surgeries for the correction of scoliosis involve an invasive intervention leading to the fusion of instrumented vertebrae. A long and painful recovery period follows the surgery and a major aesthetic trauma remains for patients [1]. Consequently, several fusionless minimally invasive surgical techniques are under development. The correction of AIS via growth modulation approaches [1–6] is promising. One of these approaches consists of inserting a small staple at the junction of the intervertebral disk and the growth plate (the region where bone growth takes place) to provide passive resistance and locally induce a corrective growth modulation [4,6]. The positioning of the staple is critical to the efficiency of the intervention [6]. This involves the precise localization of sub-surface musculoskeletal structures such as growth plates, intervertebral disks and vertebral bodies. In humans, growth plates are located on the end-plates of vertebrae next to the intervertebral disk and are mainly composed of cartilage surrounded by a fibrous ring [7].

Optical coherence tomography (OCT) is an optical imaging technique that provides non-invasive cross-sectional images of tissues to a depth of a few millimeters with a resolution ranging from 3 to 20 μm [8,9]. OCT uses low-coherence interferometry to provide depth profiles of a sample's reflectivity in real-time and with a high signal-to-noise (SNR) ratio. The technique is compatible with in vivo endoscopy as it can be performed through fiber-based catheters [9]. The use of OCT for musculoskeletal imaging has been reported for osteoarthritis monitoring where it is used to image the bone-cartilage interface and to evaluate the collagen organization of articular cartilage [10–17]. Moreover, the development of OCT handheld probes has enabled in vivo visualization of structural changes in cartilage [16,17]. These developments suggest that OCT is a good candidate for intraoperative identification of growth plates, intervertebral disks and vertebral bodies during the installation of fusionless devices.

In this study, the intrinsic contrast of OCT images was assessed in an ex vivo porcine model in order to develop an endoscopic imaging procedure for intraoperative identification of growth plates. We herein present the results of this imaging study in addition to those of the

#160161 - $15.00 USD Received 19 Dec 2011; revised 1 Feb 2012; accepted 4 Feb 2012; published 13 Feb 2012

implementation of an automated segmentation algorithm of the growth plates based on attenuation analysis.

2. Materials and methods

To assess OCT contrast of musculoskeletal tissues, porcine vertebrae were imaged and resulting OCT images were compared to corresponding histological sections. In orthopaedics, porcine models are often used to validate experimental surgical procedures as the growth rate, size and anatomy of the piglet are similar to those of juvenile and adolescent humans [1,5]. In addition, swine, like most mammals, present a second ossification center between growth plates and intervertebral disks. Small variations between human and porcine vertebrae anatomy do exist, however, it is believed that the composition of their tissues is similar [18], suggesting comparable OCT contrasts.

2.1. Imaging procedure

Freshly excised 6 months old porcine vertebrae were imaged using a commercial swept-source OCT (SS-OCT) microscope (Thorlabs, NJ, USA, discontinued). This system includes a laser source centered at 1325 nm with a spectral bandwidth of 100 nm providing an average output power of 10 mW at the sample. Images are acquired at a rate of 25 fps (i.e. 12,800 A-lines/s) and axial and transverse resolutions are 12 and 15 µm respectively. As shown on Fig. 1(a), vertebrae were imaged along an axis passing through the growth plate and volumetric data were acquired. With a fine needle, two India ink marks were positioned on each side of the growth plate on the imaging axis (Fig. 1(b)). These fiducial markers indicate the margins of the region of interest and were used to guide the histological preparation of the samples in order to validate structures seen on OCT images. Immediately after imaging, each sample was immersed in a 10% neutral buffered formalin solution for fixation. Samples were kept refrigerated between the time of sacrifice and the imaging session. The imaging procedure time from the excision of the vertebra from the spine to the fixation was approximately 30 minutes.

2.2. Preparation of histological sections

After fixation, the samples were decalcified, embedded in paraffin and cut in sections of 5 µm along the axis formed by the fiducial markers. This procedure allows a morphological correlation between images obtained with the two modalities. Histological sections were stained with H&E and Safranin O before being imaged with an optical microscope (Stemi 2000-C, Carl Zeiss, Germany).

2.3. Quantification of relative attenuation coefficients

In order to further characterize the spinal tissues of interest with OCT, relative attenuation coefficients were measured on 10 sections of spine, each taken from a different porcine specimen. Measurements consisted in evaluating the attenuation of OCT signal as a function of depth for growth plates and bones (9 samples), intervertebral disks (8 samples) and for layers of connective tissue covering the vertebrae (8 samples). To improve signal-to-noise ratio and remove speckle noise, 6 consecutive B-scans of a same volume set were averaged. From this slice, 50 A-lines were averaged (totaling an average of 300 A-lines) to obtain an attenuation profile (OCT signal versus depth). To account for topology, A-line averaging was performed after each A-line was shifted up or down to align the air-tissue interface. Each profile was plotted as the logarithm of the intensity as a function of depth and the pixels delimiting the region of interest were identified manually. The slope of the best linear fit of each curve was computed and normalized according to the maximum intensity belonging to the studied tissue. A factor of 2 was included to account for light round trip within the tissue of interest. This value represents a relative attenuation coefficient corresponding to the decay of the OCT signal with increasing depth according to Beer's law. This method was previously described by McLaughlin *et al*. and used to identify optical property variations between pathological and normal tissues [19]. For growth plate and bone, coefficients were measured

#160161 - $15.00 USD Received 19 Dec 2011; revised 1 Feb 2012; accepted 4 Feb 2012; published 13 Feb 2012

with and without the layer of connective tissue covering those structures: after imaging each intact vertebra, this layer was removed with a scalpel to unequivocally identify the position of the growth plate on OCT images. India ink markers were used as described previously to correlate images from both 3D OCT acquisitions. A non-parametric t-test was used to compare relative attenuation coefficients of the growth plates to those of the surrounding tissues.

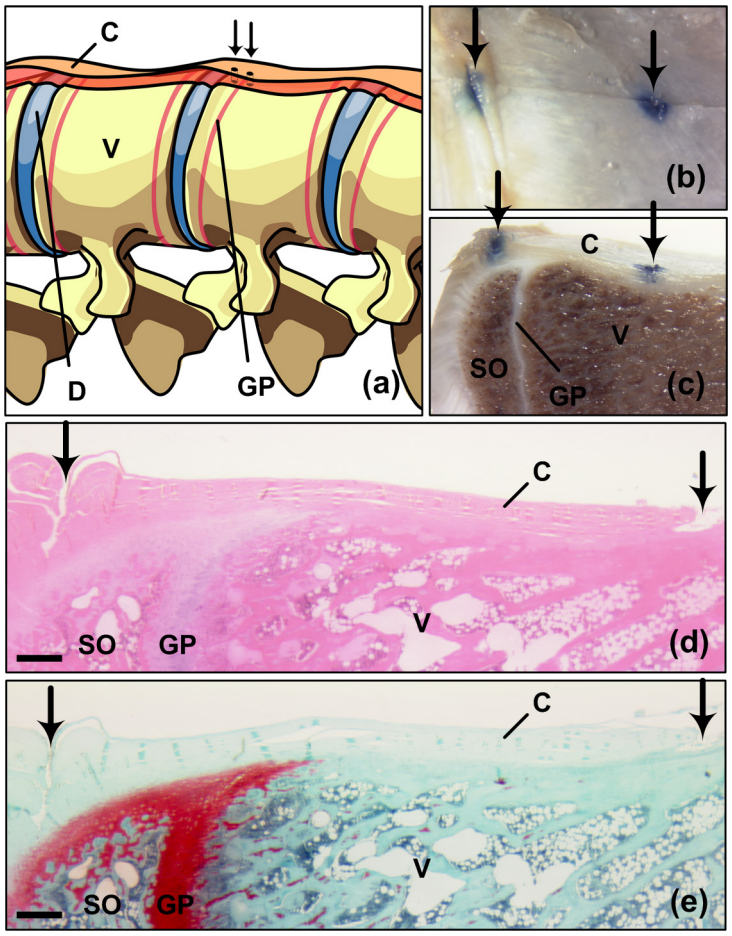

Fig. 1. Spinal structures. (a) Schematic of a spinal section showing vertebral bodies (V), intervertebral disks (D) and growth plates (GP). The arrows point at India ink marks that were performed on each side of the growth plate through a layer of connective tissue (C) to correlate histology sections ((d) and (e)) with OCT images. Pictures of (b) a top view and (c) a cut section of a marked sample covered by a layer of connective tissue. Corresponding (d) H&E and (e) Safranin O stained histological sections showing fiducial markers (arrows). SO: second ossification center. The intervertebral disk was not present on histological sections. Scale bars: 0.5 mm.

3. Imaging results

3.1. Correspondence between OCT and histological sections

Figure 2(a) shows a Safranin O stained histological section of a porcine vertebra where a superficial layer of connective tissue (~400 µm – and covering all spinal structures) has been removed to initially facilitate the identification of the growth plate. Figure 2(b) represents the corresponding OCT image. Fiducial markers visible on both the OCT section and the histological section (highlighted by arrows) allowed accurate determination of the growth

#160161 - $15.00 USD Received 19 Dec 2011; revised 1 Feb 2012; accepted 4 Feb 2012; published 13 Feb 2012

plate and bone locations. The signal attenuation as a function of depth is weaker at the location of the growth plate compared to the surrounding bone sites (corresponding to the vertebral body to the right and the second ossification center to the left). Figures 2(a) and 2(b) also show a thickening of the connective tissue layer on the left side of the image where the second ossification center meets the intervertebral disk (not shown). At this point, the signal decay is non-monotonic and creates a banding pattern which is consistent with polarization changes occurring as light passes through the collagen-rich connective tissue layer [13].

Figures 2(c) and 2(d) show the histological and OCT sections of an intact porcine vertebra sample, i.e. a sample for which the layer of connective tissue covering spinal structures was not altered. This connective tissue layer can be identified on the OCT image by its clear interface with bone tissue and by the banding pattern consistent with polarization changes due to the tissue birefringence. Despite attenuation from this superficial layer, the interface between the bone and the growth plate (highlighted by oblique arrows) remains identifiable. The second ossification center, between the growth plate and the vertebral end-plate, is however obscured on this sample by the extension of the growth plate seen on the histological section (Fig. 2(d)).

3.2. Relative attenuation coefficient measurements

Relative attenuation coefficients were measured in several sites of porcine vertebrae including growth plates, osseous tissue, intervertebral disks and connective tissue using an average of 50 consecutive A-lines from a slide composed of 6 consecutive frames. These A-lines come from regions of interest as shown in Figs. 3(d) and 3(e). Figures 3(a)–3(c) show typical A-lines for growth plate, intervertebral disk and bone, respectively. These profiles demonstrate the OCT signal differences between the musculoskeletal tissues of interest. Signal from growth plate and bone is monotonically decaying and can be fitted with a linear regression while for the intervertebral disk, the lamellar morphology is clearly observed. For measurements within the intervertebral disk region, linear fits were performed using only points corresponding to each local maximum as identified by red asterisks on Fig. 3(b). Figure 3(f) shows average relative attenuation coefficients along with their standard error on the mean. Non-parametric t-tests were used to compare measured relative attenuation coefficients with each other. Coefficients were first compared between intact and modified samples (without connective tissue) for both growth plate and bone and showed no statistical difference. This result indicates that attenuation from the connective tissue layer had no significant impact on the measurement. Coefficients for different tissues from intact samples were also compared to that of the growth plate. For each structure, there was a significant difference ($p \leq 0.05$) in attenuation compared to that of growth plate, suggesting that this measurement may be used to automatically segment growth plates on intact vertebrae with OCT data.

#160161 - $15.00 USD Received 19 Dec 2011; revised 1 Feb 2012; accepted 4 Feb 2012; published 13 Feb 2012

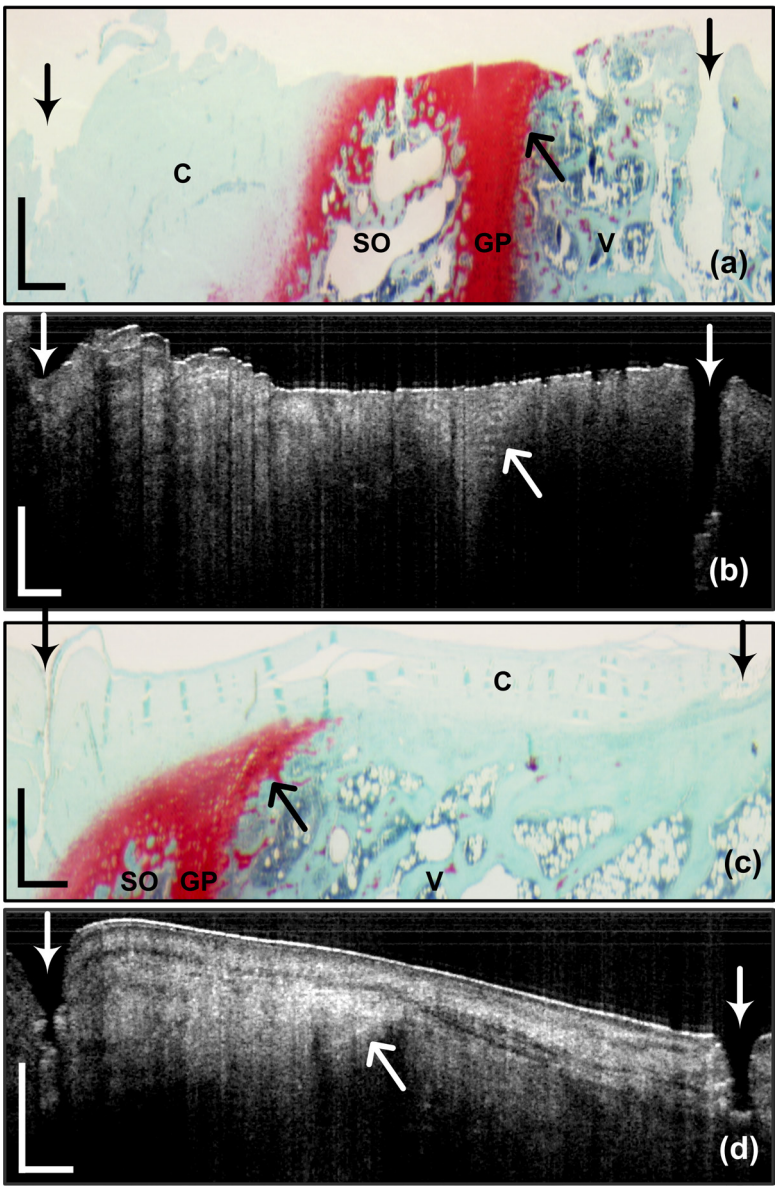

Fig. 2. Comparison of Safranin O stained ((a) and (c)) histological sections with corresponding ((b) and (d)) OCT images. (a) and (b) show the growth plate-bone interface (oblique arrows) for a modified sample (i.e. without the superficial connective tissue layer). (c) and (d) show the same interface on an intact sample. Straight arrows show the fiducial markers (India ink dots) in all images and oblique arrows highlight the growth plate-bone interface. Vertical and horizontal scale bars: 0.5 mm.

#160161 - $15.00 USD Received 19 Dec 2011; revised 1 Feb 2012; accepted 4 Feb 2012; published 13 Feb 2012

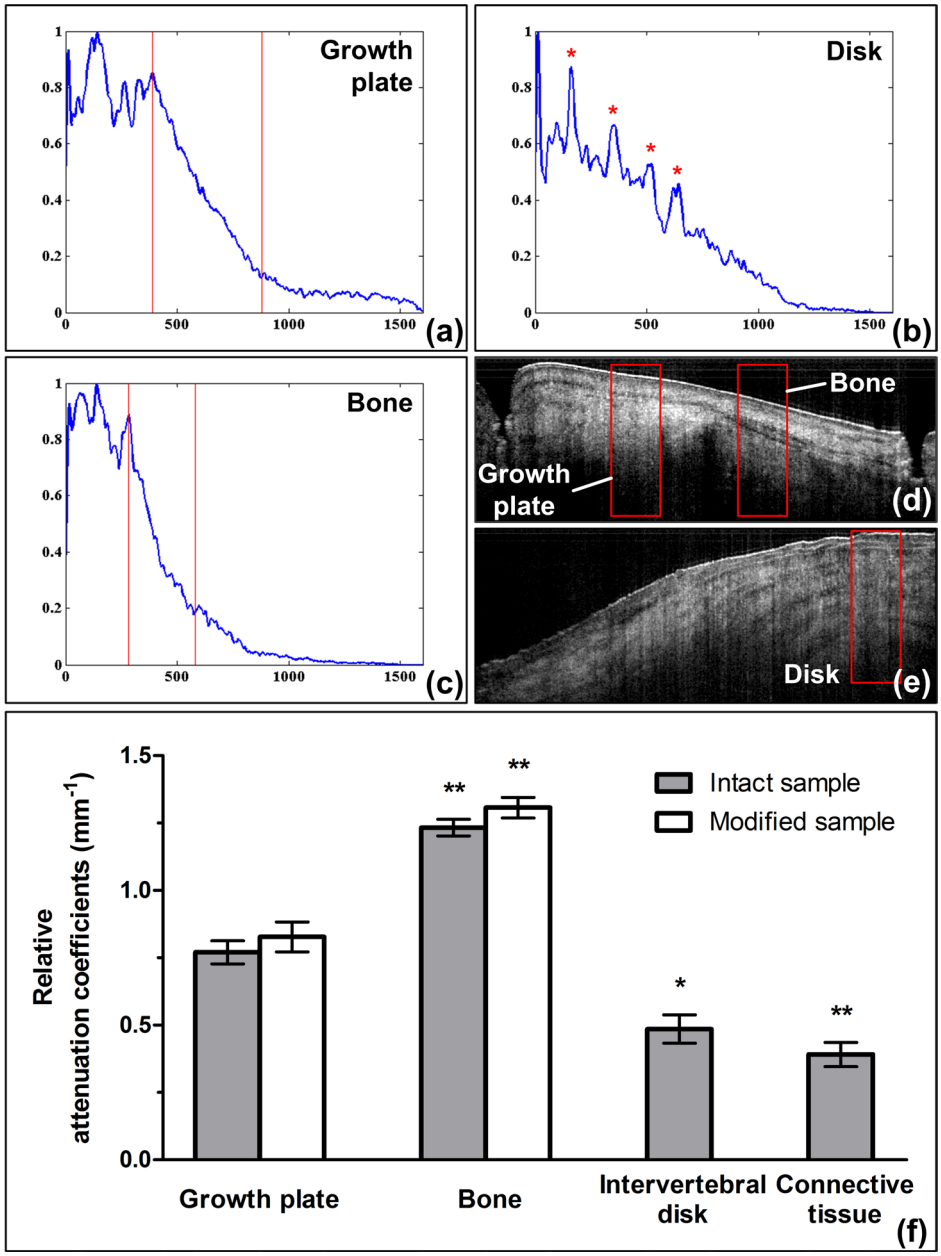

Fig. 3. Measurements of the relative attenuation coefficients. (a)-(c) Averaged and normalized A-lines (plotted as the logarithm of the OCT signal as a function of depth in microns) for a growth plate, an intervertebral disk and an osseous region, respectively. In (a) and (c), the region of interest within the A-line is delimited by red lines. In (b), red asterisks highlight the local maxima used to measure the slope of the profile. Typical set of A-lines ((d) and (e)) used to obtain attenuation profiles. (f) Histogram showing the mean attenuation coefficient for growth plate, bone, intervertebral disk and connective tissue. Error bars correspond to standard errors on the mean. Measurements in gray were obtained from intact tissue. Attenuation coefficients were also obtained for bone and growth plate without connective tissue layer (white). Relative attenuation coefficients were compared to those of growth plates; values from intact and modified samples were compared with each other ($n \geq 8$, ** $p < 0.001$ and * $p < 0.05$).

#160161 - $15.00 USD Received 19 Dec 2011; revised 1 Feb 2012; accepted 4 Feb 2012; published 13 Feb 2012

4. Preliminary implementation of an automatic growth plate segmentation algorithm

In this section, a segmentation algorithm is developed using the relative attenuation coefficients measured in Section 3. The algorithm was validated on a specimen that was not included in the set used to measure the coefficients.

4.1. Description of the algorithm

To demonstrate the utility of relative attenuation coefficients to segment growth plates on musculoskeletal tissues, an automatic detection algorithm was developed and implemented. The algorithm analyzed each A-line to measure the relative attenuation coefficient of the tissue beneath the connective tissue layer. First, 3D averaging was performed with 41 x 41 A-lines centered on the A-line of interest accounting for topology variations as described previously. The selected number of A-lines reflects a compromise between improved SNR and reduced layer localization. The resulting averaged A-line was then normalized such that the logarithm of the intensity was scaled between 0 and 1. Linear regression was performed on the averaged A-line between an upper limit (defined as the interface between the connective tissue layer and the tissue of interest) and a lower limit (defined as the point where the signal dropped to 10% of the averaged A-line maximum value). The interface between the connective tissue layer and the spinal structures was set by minimizing the error between the linear fit and the logarithmic intensity plot while maximizing the number of points used for the linear fit. The coefficient was calculated from the slope of the linear regression as described previously.

An additional criterion related to the minimal intensity reflected by the analyzed tissue was added to the algorithm. Indeed, when the value of the intensity of the first pixel of the fit was below a certain threshold, the relative attenuation coefficient was fixed at a null value. This criterion ensures that enough points are available for the fit in addition to detecting bone region with a strong attenuation coefficient. Results were displayed using a red binary image overlaid on the *en-face* projection of the OCT volume, as shown in Fig. 4(a). For relative attenuation coefficients between 0.62 and 1.05 mm^{-1}, a value of 1 was given to the binary image and corresponded to an A-line within the growth plate region. This range corresponds to that of growth plates according to the ex vivo study presented previously.

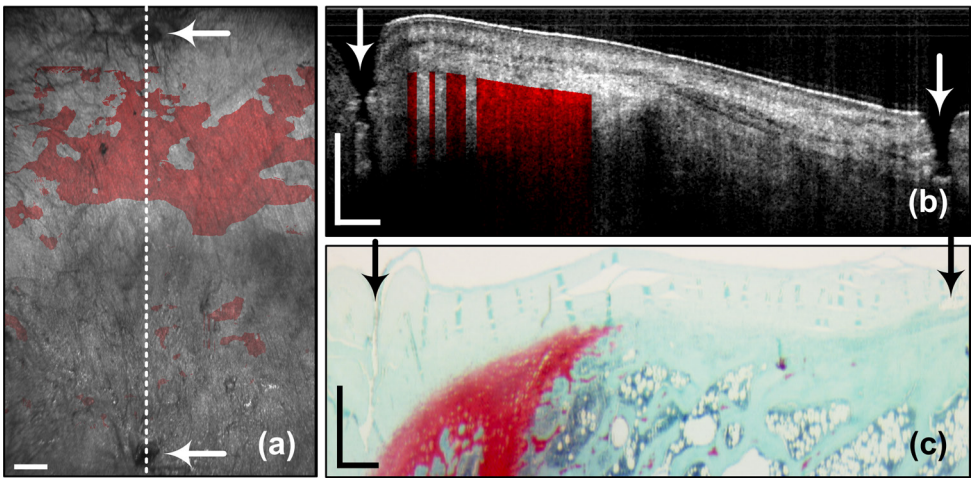

Fig. 4. Automatic growth plate segmentation algorithm. (a) Reconstructed *en-face* projection of the OCT volume of a porcine vertebra. The red region highlights the location of the growth plate. (b) shows an OCT section (identified in (a) as a white dash line) with its corresponding histological section (c). Arrows point at fiducial markers. Scale bars: 0.5 mm.

#160161 - $15.00 USD Received 19 Dec 2011; revised 1 Feb 2012; accepted 4 Feb 2012; published 13 Feb 2012

4.2. Growth plate segmentation: preliminary results

Figure 4(a) shows an *en-face* sum projection of the OCT volumetric data set combined with results from the automated growth plate segmentation algorithm. The projection is oriented so that the vertebra-disk interface is at the top of the image. As mentioned previously, red regions correspond to tissues that have been identified as growth plate by the algorithm. Figures 4(b) and 4(c) are, respectively, a frame extracted from the OCT volume and its corresponding Safranin O histological section. A-lines exhibiting attenuation coefficient in the above mentioned range were identified as growth plate and shown in red on the OCT section.

5. Discussion

This study assesses the potential of OCT for differentiating spinal tissues. In this work, we showed that OCT provides sufficient optical contrast to identify growth plates and distinguish between different spinal tissues, whether growth plates, surrounding soft/connective tissues, bone or intervertebral disks. OCT could overcome limitations associated with actual surgical guiding technique by providing an intraoperative real-time imaging modality for sub-surface growth plate identification without the use of ionizing radiation. Indeed, previous experimental surgical techniques involving insertion of growth modulation devices and requiring the localization of growth plates used fluoroscopic imaging guidance [4]. Such an imaging method lacks real-time capability as it only provides surgeons with snapshots at different time points during the procedure. Additionally, the use of x-rays requires protective clothing for the surgical team and exposes the patient to small radiation doses.

Through ex vivo imaging of porcine vertebrae, we highlighted distinctive features allowing a visual identification of musculoskeletal structures that were confirmed through histological correlations. Inherent birefringence of connective tissues introduces a band pattern that can be observed on OCT images. Birefringence in cartilaginous tissues has already been observed in osteoarthritis studies and is known to be related to the collagen matrix organization. Several studies have shown that the use of banding pattern or polarization sensitive changes can be used as a reliable marker to diagnose articular cartilage degeneration [11,13,15,17]. This band pattern could also be seen on a limited number of specimens in the growth plate, albeit with a very small visibility. Growth plate and bone were typically characterized by a monotonically decaying OCT signal having different attenuation coefficient values. The lamellar morphology of intervertebral disks made it very recognizable among other structures. Imaging of the intact vertebra suggests that OCT has an adequate penetration depth for the visualization of growth plates underneath a connective tissue layer, albeit on a porcine model.

In addition to morphological features, we also showed that relative attenuation coefficients can be used as an additional contrast mechanism to differentiate musculoskeletal structures. The use of attenuation measurements to enhance tissue contrast on OCT images has been previously assessed for cardiovascular [20,21] and oncological applications [19]. We quantified the signal attenuation for some musculoskeletal tissues of the spine showing that growth plates present a distinctive relative attenuation coefficient range when compared to surrounding tissues. Osseous tissues had the strongest attenuation coefficient which may be explained by a strong absorption from red blood cell precursors in the bone marrow.

Relative attenuation coefficients measured in this study did not account for the influence of the confocal properties of the system as depth of focus and the position of the focus in the sample. Absolute values of attenuation coefficients can be extracted from OCT data by accounting for these parameters with a more complex model as shown by van der Meer *et al*. [20]. Relative attenuation coefficients are however easier to calculate and relevant from a clinical perspective. In our case, only relative changes of optical properties are required to distinguish between different types of tissues. A calibration procedure may however be necessary when different acquisition systems are used.

An automatic segmentation algorithm was further implemented to demonstrate the potential of signal attenuation quantification for the identification of growth plates on OCT

#160161 - $15.00 USD Received 19 Dec 2011; revised 1 Feb 2012; accepted 4 Feb 2012; published 13 Feb 2012

images. The algorithm successfully identified the growth plate on an OCT volume of a porcine vertebra amidst bone and intervertebral disk tissues. This algorithm could easily be added to an OCT acquisition software to provide surgeons with additional real-time information. This simple algorithm correctly identified the growth plate on our samples. However, testing it on a larger data set would be required to calculate sensitivity and specificity ratios.

Some limitations have been identified. In the *en-face* projection, one can see that some regions of the bone have been erroneously identified as growth plate tissues. The analysis of the erroneous attributions showed two main reasons of these failures. First, the limit between the connective tissue layer and underlying tissues was not always properly assessed. Second, in transition regions where growth plate and bone overlap, the computed monotonic relative attenuation coefficient was indeed erroneous. To overcome these limitations further improvement on the algorithm will allow for multiple decay rates when two monotonic decays do not fit the data. Moreover, combining relative attenuation coefficient with other OCT contrast mechanisms as banding pattern due to birefringence and lamellar morphology will certainly enable a good segmentation of all musculoskeletal structures.

Future investigations include using these results in vivo on a porcine model with a handheld OCT probe. Longer wavelength could also be investigated towards improving the growth plate detection depth [22,23].

Acknowledgments

The authors thank Emre Aslan, Liane Bernstein, Étienne de Montigny and Romain Deterre for their valuable suggestions and precious laboratory help, in addition to Professor Caroline Hoemann for her histology services. This work was funded by NSERC (Natural Sciences and Engineering Research Council of Canada) and CFI (Canadian Foundation for Innovation). Kathy Beaudette and Mathias Strupler are funded through Fondation CHU Ste-Justine and Fondation des Étoiles.

#160161 - $15.00 USD Received 19 Dec 2011; revised 1 Feb 2012; accepted 4 Feb 2012; published 13 Feb 2012